



AirCargoChallenge 2022

Technical Report

Team #11

ITU SKY UAV





Table of Contents

1. INTRODUCTION	5
1.1. EXECUTIVE SUMMARY	5
1.1.1. Design Process	5
1.1.2. Mission Requirements and Constraints	5
2. PROJECT MANAGEMENT	6
2.1. Team Organisation.....	6
2.2. Time Scheduling.....	6
2.3. Financial Budget.....	7
3. AERODYNAMIC DESIGN	7
3.1. Wing Planform Configurations	7
3.2. Wing Vertical Position Configurations	8
3.3. Tail Configurations	8
3.4. Landing Gear Configurations	9
3.5. Aerodynamic Design and Sizing	9
3.5.1. Airfoil Selection	9
3.5.2 Wing Design	12
3.6. Stability	12
3.6.1. Center of Gravity and Static Margin	13
3.6.2. Longitudinal Stability.....	14
3.6.3. Lateral- Directional Stability.....	16
3.7. Estimation of Drag and Thrust	17
3.7.1. Parasite Drag.....	18
3.7.1.1. Skin Friction Coefficient	18
3.7.1.2. Form Factors.....	19
3.7.2. Induced Drag.....	19
3.7.3. Crud Drag	20
3.7.4. Thrust Calculation	20
3.7.5. Drag and Thrust Calculation Results	20
3.7.6 Verification of Wing Produced Lift and Drag	21
4. STRUCTURAL DESIGN	23
4.1. Wing Structural Design	23
4.2. Tail Structural Design	25
4.3. Fuselage and Mechanical Systems	26
4.3.1. Fuselage	26

4.3.2. Mechanical Systems.....	26
4.3.3. Wings and Tail.....	26
4.3.4. Landing Gear.....	27
4.4. Wing Structural Analysis.....	27
5. AVIONICS.....	30
5.1. Batteries.....	30
5.2. ESC.....	30
5.3. Connectors.....	30
5.4. Servos.....	30
5.5. Radio Control.....	30
6. PAYLOAD PREDICTION.....	31
7. OUTLOOK.....	32
REFERENCES.....	33

List of Tables

Table 1: Financial Budget.....	7
Table 2: Center of Gravity Calculation.....	13
Table 3: Static margin calculations.....	14
Table 4: $Cd0$ calculations.....	19
Table 5: XFLR5 and ANSYS Fluent Comparison for Cl calculation.....	22
Table 6: Comparison for $Cd0$ calculations.....	22
Table 7: Fuselage Material Selection.....	26
Table 8: Wing-Tail Material Selection.....	27
Table 9: Landing Gear Material Selection.....	27

List of Figures

Figure 1: Team Organization Chart.....	6
Figure 2: Time Schedule.....	6
Figure 3: Wing Planform Configuration Selection.....	7
Figure 4: Wing Vertical Position Configuration Selection.....	8
Figure 5: Tail Configuration Selection.....	8
Figure 6: Landing Gear Configuration Selection.....	9
Figure 7: DAE 31 Airfoil achieved from XFLR5.....	10
Figure 8: E205 Airfoil achieved from XFLR5.....	10
Figure 9: FX 63-137 Airfoil achieved from XFLR5.....	10
Figure 10: Cl - α comparison of airfoils achieved from XFLR5.....	10
Figure 11: Cd - α comparison of airfoils achieved from XFLR5.....	11
Figure 12: Cm - α comparison of airfoils achieved from XFLR5.....	11
Figure 13: Cl/Cd - α comparison of airfoils achieved from XFLR5.....	11
Figure 14: Properties of final wing design.....	12

Figure 15: Types of Stability [1].....	13
Figure 16: Weigth entered in the XFLR5 program and position of center of gravity.....	13
Figure 17: Ideal Region for Center of Gravity on Aircraft [2]	14
Figure 18: Cm / alpha graph.....	15
Figure 19: Parameters of formula on sample aircraft model [2]	15
Figure 20: Tail parameters	15
Figure 21: Cn- β and Cl- β graphics achieved from XFLR5.....	16
Figure 22: Vertical Tail Dimensions	17
Figure 23: Drag versus Velocity Graph	20
Figure 24: Drag-Thrust Comparison	21
Figure 25: Contribution to drag of aircraft components.....	21
Figure 26: CFD Results for Cl calculation from ANSYS Fluent	22
Figure 27: CFD Results for Cd calculation from ANSYS Fluent	22
Figure 28: Streamlines for tip vortices from ANSYS Fluent.....	23
Figure 29: Streamlines on wing surface from ANSYS Fluent.....	23
Figure 30: Wing Structure	24
Figure 31: Fuselage Connection (Root Section)	24
Figure 32: Connections View From Above	25
Figure 33: Tail internal structure and control surfaces.....	25
Figure 34: Shrenk Approximation results and calculated lift distribution over wing	28
Figure 35: Lift distribution over wing surface for Schrenk Approximation.....	29
Figure 36: The Finite Element Model with Applied Forces in the MSC Patran	29
Figure 37: The displacement results for static analysis obtained by MSC NASTRAN	29
Figure 38: Payload prediction graphic.....	31
Figure 39: Side view of final aircraft.....	32
Figure 40: Isometric view of final aircraft	32



1.INTRODUCTION

1.1. EXECUTIVE SUMMARY

This report details the design process, analysis, manufacturing, and testing plans of the ITU SKY UAV Team from Istanbul Technical University for the Air Cargo Challenge 2022. The aim of the Air Cargo Challenge competition is to carry the blood bags, which are medical emergency goods, as much as possible within the specified time and to travel as far as possible with the blood bags. The team aimed to achieve the maximum payload weight. The team designed the UAV by complying with the constraints specified in the regulation. According to the results of the analyses and designs, the UAV will have a high wing and a conventional tail type.

1.1.1. Design Process

At the beginning of the design process, the team estimated the UAV's total weight and determined the payload weight to be carried. During the preliminary design phase, the aim is for the aircraft to be subjected to the least amount of drag and produce the maximum lift force during flight. To achieve this goal, it was tried to select an aerodynamically efficient airfoil. One of the criteria for the design is that the aircraft take off from a short distance as specified in the regulation. In addition, it has been taken into account that the aircraft also has sufficient maneuverability to turn sharp corners. The avionic elements that will be used in the aircraft are the LiPo battery, receiver, ESC, and GPS.

1.1.2. Mission Requirements and Constraints

The total time determined for flights in the Air Cargo Challenge competition is 180 seconds. The first 60 seconds of this time will be spent for the aircraft to achieve altitude, and after 60 seconds, the altitude will be recorded. Then, at the end of the remaining 120 seconds, the total distance traveled by the aircraft will be recorded. The main task is to carry as much weight as possible to the longest distance. In addition, fast mounting of the payload on the aircraft and removal also earn points.

There are some challenging conditions in the competition. The first of these conditions is that the takeoff distance should not exceed 60 meters. Secondly, according to airworthiness rules, the maximum altitude that the aircraft can reach is 120 meters. In addition, the disassembled version of the aircraft fits in a 110 x 25 x 40 cm box, and the assembled aircraft must fit into a rhombus-shaped box with an edge length of 1.5 m each. 50 cm is the maximum height for the assembled aircraft.

2. PROJECT MANAGEMENT

2.1. Team Organisation

The team consists of 20 undergraduate students. Team members took on tasks according to their interests and abilities during the design and production phase of the aircraft. The work was divided during the design phase into Aerodynamics, CAD and Structures, Avionics and Manufacturing. During the design phase, the design was carried out more efficiently with the active communication and cooperation of team members working on different fields.

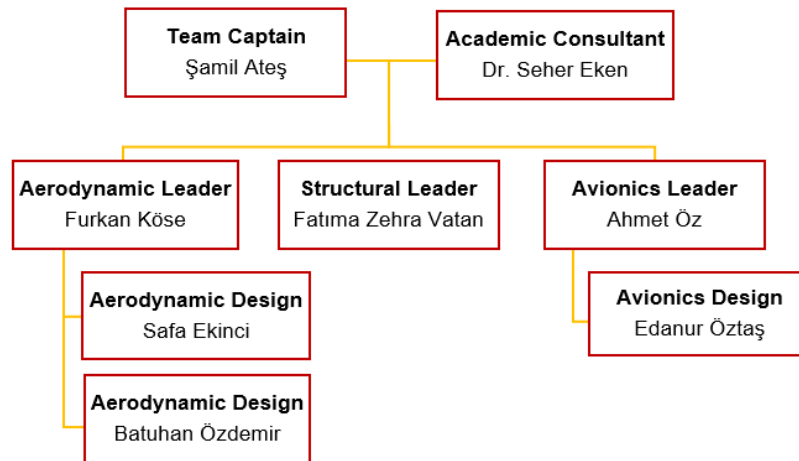


Figure 1: Team Organization Chart

2.2. Time Scheduling

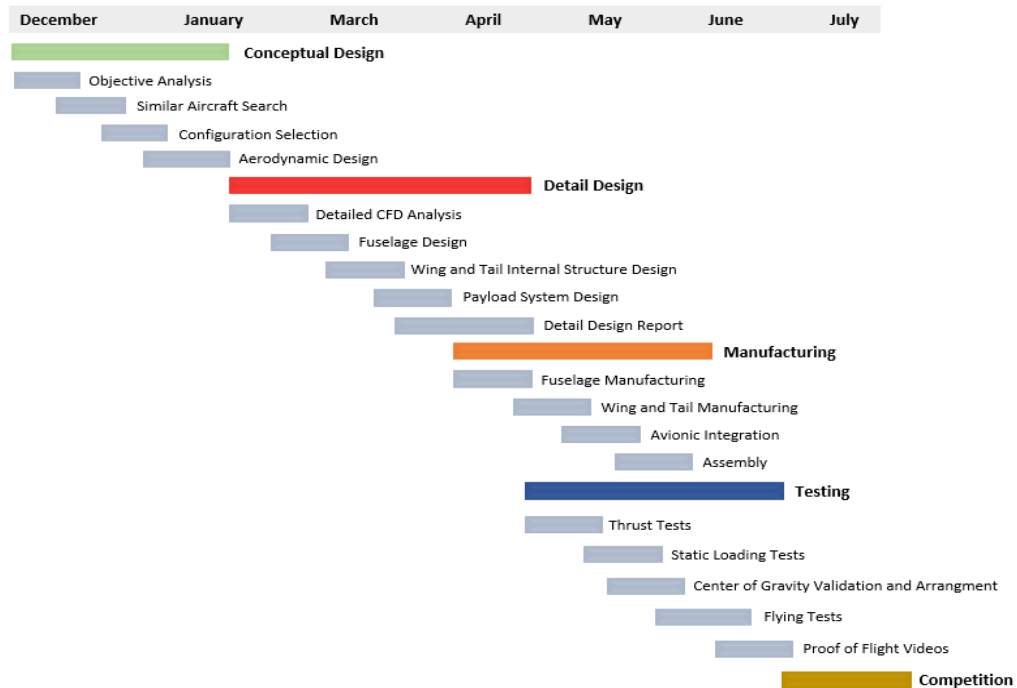


Figure 2: Time Schedule

The time schedule prepared by the team can be seen in Figure 2. The team aims to work hard by complying with the timeline to overcome challenges that may occur during the production and testing phase.

2.3. Financial Budget

Table 1: Financial Budget

No	Item	Unit Price	Quantity	Total Price
1	Balsa	TRY 60	25	TRY 1500
2	Plywood	TRY 325	2	TRY 650
3	Carbon Pipe	TRY 100	12	TRY 1200
4	Covering Film	TRY 110	8	TRY 880
5	Epoxy	TRY 375	2	TRY 750
6	Motor	TRY 1900	1	TRY 1900
7	Propellers	TRY 45	1	TRY 45
8	ESC	TRY 325	1	TRY 325
9	Batteries	TRY 1300	1	TRY 1300
10	Filament	TRY 200	2	TRY 400
11	Tools	TRY 150	8	TRY 1200
12	Landing Gear	TRY 400	2	TRY 800
13	Fasteners	TRY 10	10	TRY 100
	Total			TRY 11050

3. AERODYNAMIC DESIGN

3.1. Wing Planform Configurations



Criteria	Coefficient	Rectangular Wing	Tapered Wing	Elliptical Wing
Lift	0,25	7	9	10
Stability	0,2	10	8	6
Manufacturability	0,2	10	9	6
Size Restriction	0,15	6	10	9
Maneuverability	0,1	7	9	10
Drag	0,1	9	8	5
Total	1	8.25	8.85	7.75

Figure 3: Wing Planform Configuration Selection

The tapered wing is preferred as the wing planform because of the fact that the tapered wing is more aerodynamically efficient than the rectangular wing and easier to manufacture than the elliptical wing. Also, the use of tapered wings enabled us to achieve the needed aspect ratio that will ensure wing area to produce the demanded lift and enough maneuverability while allowing the aircraft to fit into the rhombus-shaped box specified in the competition regulations.

3.2. Wing Vertical Position Configurations

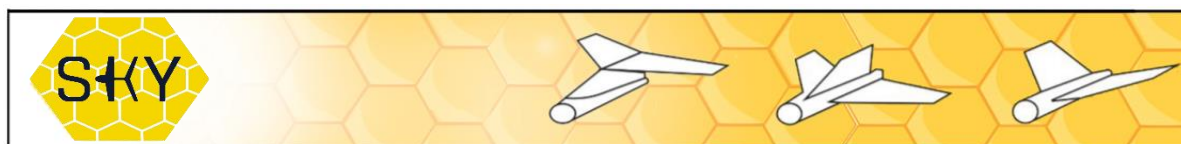


Criteria	Coefficient	High Wing	Mid Wing	Low Wing
Lift	0.4	10	9	8
Stability	0.25	10	8	9
Drag	0,2	8	9	8
Maneuverability	0,15	7	9	8
Total	1	9.15	8.75	8.25

Figure 4: Wing Vertical Position Configuration Selection

Due to competition regulations, the lift force required to carry as much payload as possible, as well as the requirement to place a payload box inside the fuselage, were the primary criteria considered. The wing configuration was chosen for several reasons: the high wing configuration generates the most lift force, the location of the center of gravity being below the wing causes the fuselage to act as a pendulum during roll moments, which increases lateral stability, and the wing-to-fuselage fasteners being high on the fuselage's vertical axis makes it easier to position the payload inside.

3.3. Tail Configurations

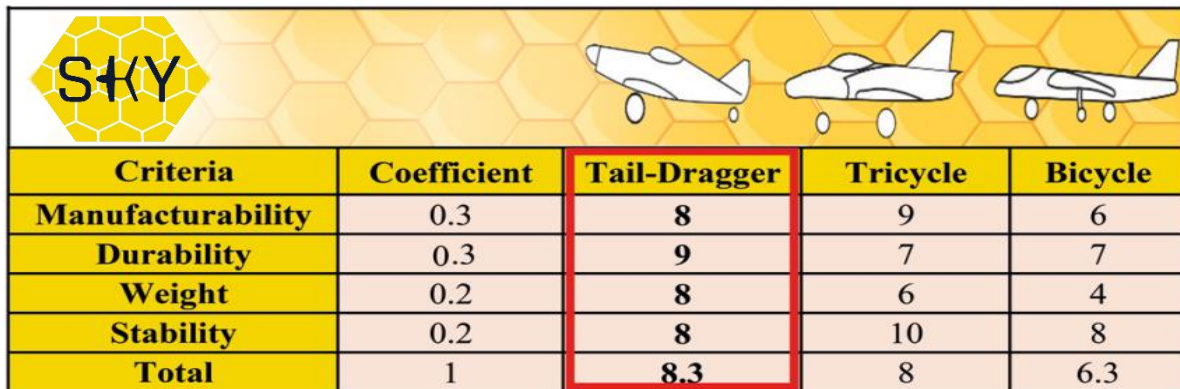


Criteria	Coefficient	T-Tail	Conventional Tail	V-Tail
Controllability	0.4	9	8	6
Manufacturability	0.3	7	10	5
Weight	0.2	8	8	9
Drag	0.1	9	8	8
Total	1	8.2	8.6	6.5

Figure 5: Tail Configuration Selection

T-tail, V-tail, and conventional tail are the most commonly used among UAVs for comparable purposes. In order to obtain the necessary trim and stability conditions, a conventional tail was preferred. Ease of production compared to other tail configurations and high controllability were the main reasons for the decision to use a conventional tail.

3.4. Landing Gear Configurations



Criteria	Coefficient	Tail-Dragger	Tricycle	Bicycle
Manufacturability	0.3	8	9	6
Durability	0.3	9	7	7
Weight	0.2	8	6	4
Stability	0.2	8	10	8
Total	1	8.3	8	6.3

Figure 6: Landing Gear Configuration Selection

In the determination process of landing gear type, the most important factor is considered as the landing and take-off safety. Since tail-draggers are the safest due to the motor being located high, it was decided to use a tail-dragger to minimize the damage that can be taken during landing and take-off. Also, tail-dragger landing gear has reduced parasitic drag and weight compared to other types which affected the determination process.

3.5. Aerodynamic Design and Sizing

Dimensions and design parameters of the main components of aircraft have been determined and discussed in this section.

3.5.1. Airfoil Selection

To sustain an aircraft's flight, the lift force required to overcome its weight and wings generate most of the lift aircraft need. Airfoil is one of the most important sides of this problem. Lift force is generated from the pressure difference between the upper and lower side of the airfoil. So, when selecting the airfoil lift force must be considered. But it is not enough just considering lift force. Keeping drag force low is important since there is a limited amount of thrust. Also keeping the moment coefficient low to maintain stable flight. There are other parameters about the selection of airfoil which are airfoil designs according to Reynolds number and camber size according to have enough space for internal parts of the wing such as spars and ribs and with a high stall angle because of climbing with a high angle of attack and $C_{l_{max}}$. Since thrust limitations we decided to fly around 12m/s so our aircraft's Reynolds number will be ≈ 215.000 . Since that low Reynolds airfoils must be selected. With these requirements we analyzed too many airfoils using the XFLR5 program. After this analysis, 3 airfoils showed high performance and we chose the best one among them.



Figure 7: DAE 31 Airfoil achieved from XFLR5

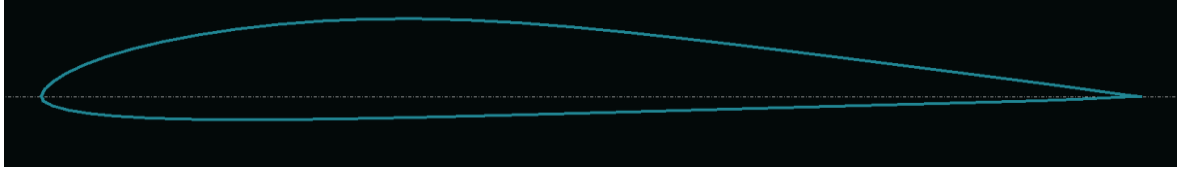


Figure 8: E205 Airfoil achieved from XFLR5

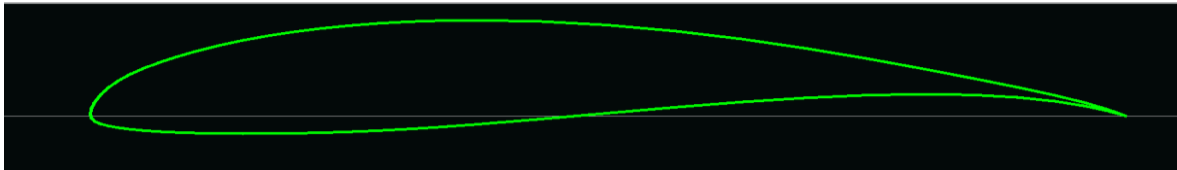


Figure 9: FX 63-137 Airfoil achieved from XFLR5

The intent of this selection process is to select an airfoil for an aircraft that is a low Reynolds number cargo UAV. Thrust is limited since the engine and propeller are set by regulations. At 12 m/s, 6.12 N of thrust is available since the selected airfoil must have a low C_d to maintain cruise flight. The selected airfoil must provide enough lift at cruise speed, so the $C_l - \alpha$ graph also must be evaluated for this concern. To find an airfoil which has optimal performance according to getting drag and enough lift, the $C_l/C_d - \alpha$ plot must be evaluated. Also, as stated above, in order to maintain stable flight, C_m is an important coefficient. So $C_m - \alpha$ graph must be considered. To get these plots, we used the XFLR5 program.

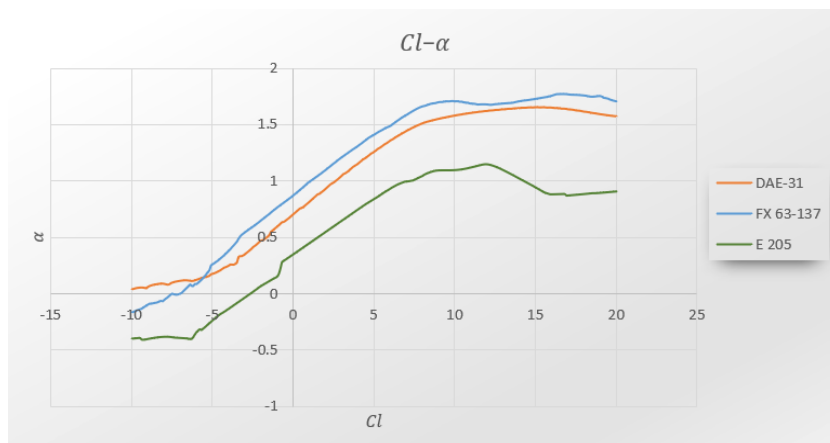


Figure 10: $C_l - \alpha$ comparison of airfoils achieved from XFLR5

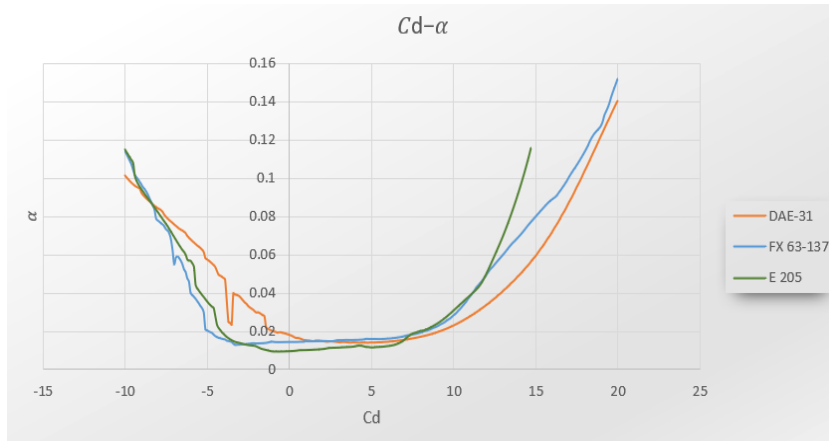


Figure 11: Cd - alpha comparison of airfoils achieved from XFLR5

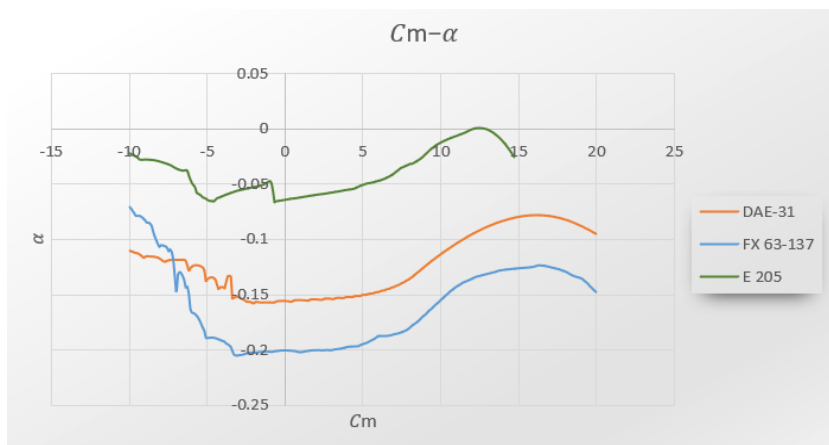


Figure 12: Cm - alpha comparison of airfoils achieved from XFLR5

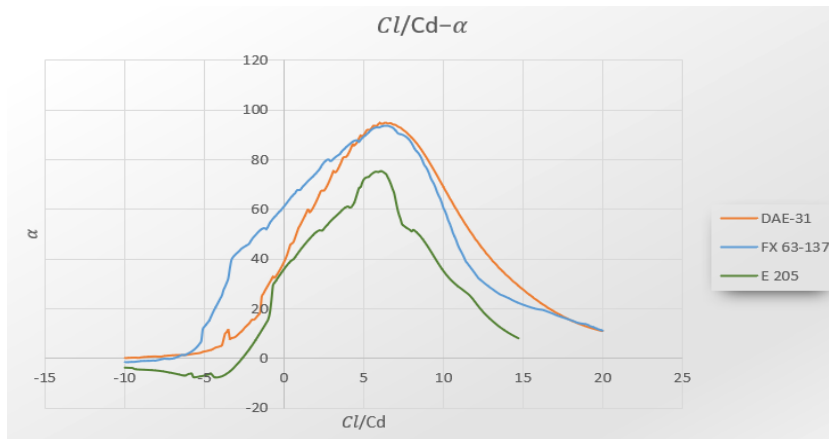


Figure 13: Cl/Cd - alpha comparison of airfoils achieved from XFLR5

According to these plots DAE-31 and FX 63-137 airfoils have higher lift and lower drag. Even FX 63-137 has better performance but it is a more cambered and thinner airfoil. Since the difference between DAE-31 and FX 63-137 is not that big enough to convince us to confront structural problems. Between DAE-31 and E 205, DAE-31 has more lift and low drag and also has low C_m . According to these evaluations we decided to continue with DAE-31.

3.5.2 Wing Design

The main aim of wing design is to acquire the lift that is needed to sustain cruise flight with the lowest possible drag force. According to regulation, the aircraft must be fitted to a rhombus shaped with 1.5 m edge length. Within these restrictions the wing must produce lift force to carry 3.2 kg total weight of the aircraft. The formula of the lift force that the wing must produce to carry this weight;

$$W = L = \frac{1}{2} \rho V^2 S_{wing} C_L$$

Using this formula to get an initial point the wing chord, sweep, dihedral, incidence and sweep distributions along the span parameters were studied using an iterative study using XFLR5.

After the design process on XFLR5 we set the design of the wing as:

Wing Span	215.00 cm
Area	5484.25 cm ²
Projected Span	215.00 cm
Projected Area	5484.25 cm ²
Mean Geom. Chord	25.51 cm
Mean Aero Chord	26.69 cm
Aspect ratio	8.43
Taper Ratio	0.46
Root to Tip Sweep	7.55 °

Figure 14: Properties of final wing design

To acquire lift to maintain level flight the wing is fitted on the plane with a 3.5° tilt angle on top of the aircraft.

3.6. Stability

Stability is defined as the ability of an aircraft to return to its flight path in the face of weather events such as turbulence or a sudden change in weather. Stability assists pilots in maintaining the specified and desired flight condition and responding to disturbances that may occur during that flight condition. There are 2 types of stability in airplanes: static and dynamic. Dynamic stability refers to the response time when disturbed by a tilt or bank movement. Static stability is the tendency of the aircraft to return to the steady-state flight condition as a result of encountering any small atmospheric disturbance in the steady-state flight condition.

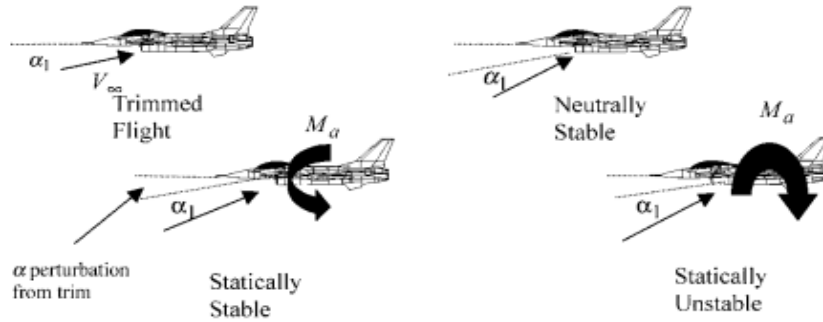


Figure 15: Types of Stability [1]

3.6.1. Center of Gravity and Static Margin

The center of gravity of an aircraft is an important location for designing a stable aircraft. To determine the location of the center of gravity we used the XFLR5 program by giving all parts of the aircraft as an input with their center of gravity locations.



Figure 16: Weight entered in the XFLR5 program and position of center of gravity

Table 2: Center of Gravity Calculation

Components							
Structural Parts				Avionic Parts			
Parts	y (mm)	Weight (g)	Moment	Parts	y (mm)	Weight (g)	Moment
Wing x 2	-230	340	-78200	Motor	275	177	48675
Blood Bag	10	1200	12000	ESC	190	63	11970
Blood Bag Box	10	40	400	Servo Motor x 2 (Wing)	-200	76	-15200
Fuselage	-75	250	-18750	Servo Motor x 2 (Elevator)	-700	76	-53200
Landing Gear (Front)	50	150	7500	Servo Motor (Rudder)	-700	38	-26600
Landing Gear (Rear)	-680	50	-34000	Receiver	-155	14	-2170
Tail - Fuselage Link	-400	50	-20000	3S Li-Po Battery	-252.5	250	-63125
Wing - Fuselage Link	-190	50	-9500	GPS Box	-327.5	150	-49125
Tail Parts	-660	250	-165000	2S Insurance Li-Po Battery	-200	53	-10600
Tail - Fuselage Pipe	-480	40	-19200	-	-	-	-
Total		Weight (g): 3317				Moment (mm*g): -484125	
Center of Gravity (mm)							-145.953

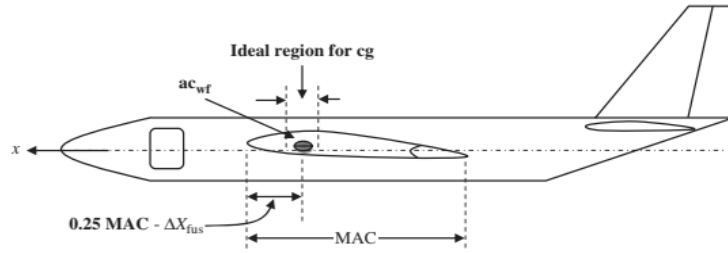


Figure 17: Ideal Region for Center of Gravity on Aircraft [2]

To examine how ideal the CG location of the aircraft is we get the aerodynamic center of the wing from the XFLR5 program. To estimate its adequacy, we used Static Margin. To obtain a longitudinally stable design static margin ($\frac{h_{ac}-h_{cg}}{c}$) must be between 0.1c - 0.3c is the mean aerodynamic chord of the wing and it is 26.68 cm.

Table 3: Static margin calculations

Parameters	Distance to Leading Edge of Wing
h_{cg}	14.3 cm
h_{ac}	17 cm
$\frac{h_{ac} - h_{cg}}{C}$	0.102

According to intentions, the static margin of the aircraft fits the requirements.

3.6.2. Longitudinal Stability

Obtaining a longitudinally stable design is an important criterion when configuring the aircraft. While making this design, the longitudinal aerodynamic center of the aircraft should be ahead of the center of gravity (closer to the nose). This will cause the cm-alpha graph to be a graph with a negative slope (Figure 19). Because any effect (deterioration or lift increase) affecting the aircraft will increase the lift of the aircraft. This increase in force will occur at the aerodynamic center. Considering this increase, when the moment balance with respect to the CG is written, it will force the aircraft to 'pitch up'. In order to balance this movement, there will be an increase in the lift in the horizontal tail, and when the moment is taken according to the CG by using this increase in the force, the pitch moment balance of the aircraft must be ensured by forcing the "pitch down" movement. The mentioned moment balance is expressed with the following sets of equations, and the horizontal tail is designed by adhering to the following set of equations after the design of the wing;

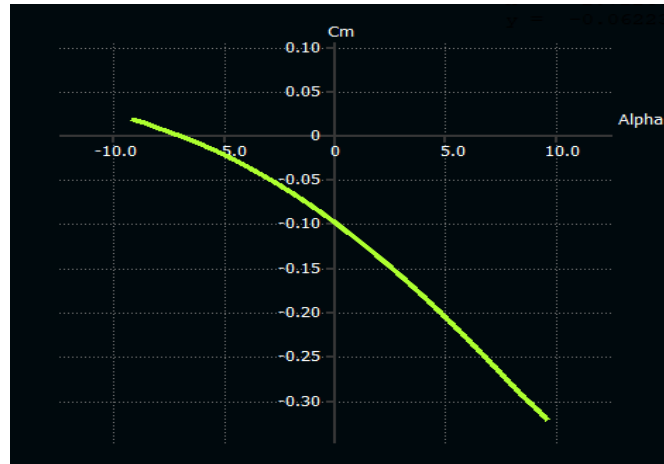


Figure 18: C_m / α graph

$$\sum M_{cg} = 0 \rightarrow M_{0_{wf}} + M_{L_{wf}} + M_{L_h} + M_{0_h} + M_{T_{eng}} + M_{D_w} = 0$$

$$C_{m_{0_{wf}}} + C_L(h - h_0) - \eta_h \bar{V}_h C_{L_h} = 0$$

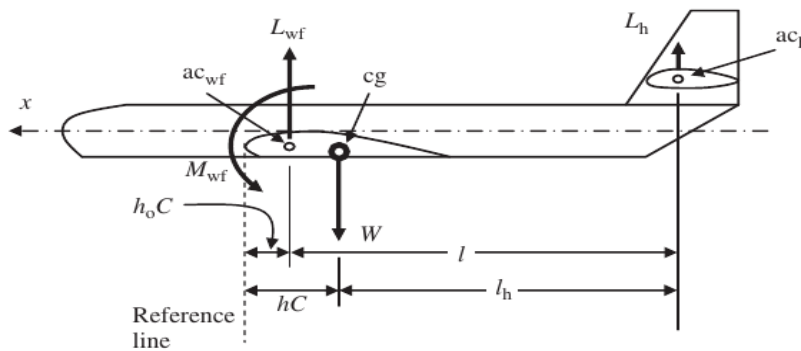


Figure 19: Parameters of formula on sample aircraft model [2]

By using the above set of equations, it is aimed to design a horizontal tail to provide longitudinal stability. With these in mind naca 0012 airfoil has used to maintain symmetry. The distance of the horizontal tail to the CG was calculated as 49.7 cm, and the remaining parameters are as follows;

Wing Span	51.00 cm
Area	1020.00 cm ²
Projected Span	51.00 cm
Projected Area	1020.00 cm ²
Mean Geom. Chord	20.00 cm
Mean Aero Chord	20.07 cm
Aspect ratio	2.55
Taper Ratio	1.22
Root to Tip Sweep	6.71 °
Number of Flaps	0
Number of VLM Panels	266
Number of 3D Panels	546



Figure 20: Tail parameters

3.6.3. Lateral- Directional Stability

While designing any aircraft, the aircraft must be symmetrical along the x-axis. Assuming that no disturbances occur, the mentioned symmetry keeps the aircraft lateral and directionally stable. However, when any lateral wind acts, a change will be observed in the side slip angle of the aircraft. This angle change will affect the lateral and directional stability of the aircraft. Since the aircraft is desired to remain in a stable position, the vertical tail and symmetrical wing-fuselage structure designed against these disturbances will tend to return the aircraft to the flight phase where it started again. For this reason, the yaw moment and roll moment behaviors of the aircraft under different side slip angle conditions were examined in the image below using the XFLR5 program. In order to provide Directional-Lateral stability, the slope of the Roll Moment-Beta graph of the aircraft must be less than 0 and the Yaw Moment-Beta graph must be greater than 0. As explained, an acting positive side slip angle will increase lift on the right wing of the airplane (as viewed from the z-axis). This increase will cause a roll moment in the -x direction. According to the graph obtained below, this event is sufficient to explain that the plane will be stable laterally when the slope is negative. Likewise, a positive side slip angle will change the lift at the vertical tail, causing a yaw moment in the +z axis. This is explained by the positivity of the C_n -Beta graph, showing that the aircraft provides directional stability

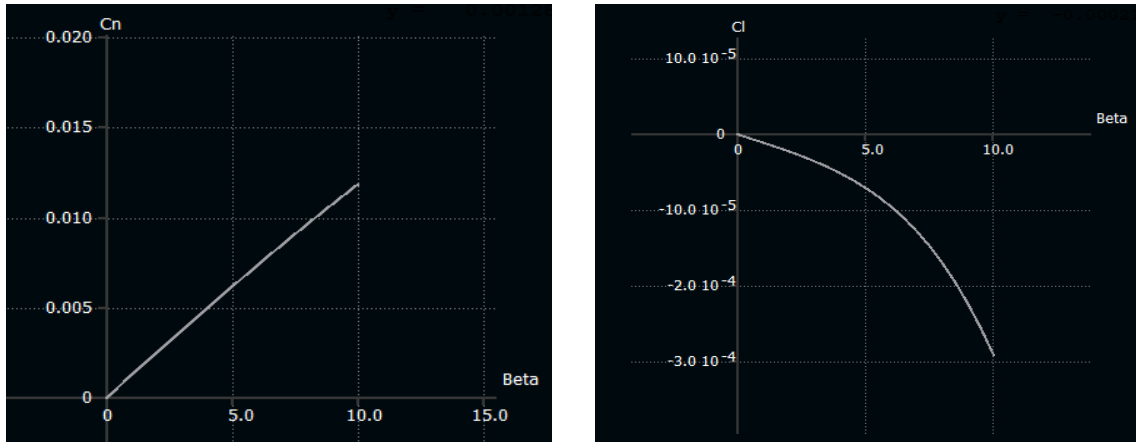


Figure 21: C_n - β and C_l - β graphics achieved from XFLR5

Mathematically, the lateral-directional stability derivatives mentioned above are explained as follows. N_A and N_T are aerodynamic yaw moment and thrust yaw moment, L_A and L_T are aerodynamic roll moment and thrust roll moment respectively.

$$\frac{\partial(N_A + N_T)}{\partial\beta} > 0$$

$$N_A + N_T = (C_n + C_{T_n})\bar{q}Sb$$

$$C_{n\beta} + C_{n\tau\beta} > 0$$

The final representation of the stability derivative, ignoring the yaw moment at which the thrust is seen, is as follows;

$$C_{n\beta} > 0$$

The equation sets for side slip angle and Roll moment are as follows;

$$\frac{\partial(L_A + L_T)}{\partial\beta} < 0$$

$$L_A + L_T = (C_l + C_{l\tau})\bar{q}Sb$$

$$C_{l\beta} < 0$$

With these in mind naca 0012 airfoil has used to maintain symmetry and remaining parameters of vertical tail are as follows:

Wing Span	50.00 cm
Area	562.50 cm ²
Projected Span	50.00 cm
Projected Area	562.50 cm ²
Mean Geom. Chord	22.50 cm
Mean Aero Chord	22.59 cm
Aspect ratio	2.22
Taper Ratio	1.25
Root to Tip Sweep	8.53 °
Number of Flaps	0
Number of VLM Panels	35
Number of 3D Panels	84

Figure 22: Vertical Tail Dimensions

3.7. Estimation of Drag and Thrust

Drag is the aerodynamic force that resists an aircraft's motion through the air. Every component (interacted with fluid) of the airplane generates drag. Furthermore, there must be a velocity difference between fluid and solid bodies to produce drag. During the subsonic flight, there are two forms of drag force. Those are parasite drag and induced drag. Parasite drag (a.k.a zero-lift drag) is related to the shape of the solid and its skin friction. Parasite drag affects all components, regardless of whether they can generate lift. On the other hand, induced drag occurs due to lifting surfaces.

$$D = \frac{1}{2}\rho V_{\infty}^2 S C_D$$

In addition to parasite and induced drag, we will include the term 'crud drag' for external factors such as production defects. Finally, we can calculate the drag coefficient by summing the parasite, induced and crud drag coefficients.

$$C_D = C_{D_0} + C_{D_i} + C_{D_{crud}}$$

3.7.1. Parasite Drag

Parasite drag can be estimated by using a build-up method [3].

$$(C_{D_0})_{subsonic} = \frac{\sum(C_{f_c} \cdot FF_c \cdot Q_c \cdot S_{wet})}{S_{ref}}$$

C_f = Skin friction coefficient

FF = Form factor (estimate pressure drag due to viscous separation)

Q = Interference Factor

S_{wet} = The wetted area (The total area of the component that is in contact with the fluid)

S_{ref} = The wing reference area (The top view area of the wing)

3.7.1.1. Skin Friction Coefficient

First of all, we must decide whether the piece deals with the laminar or turbulent flow. To make this decision, we should investigate the Reynolds number. As an assumption, we will take laminar flow if $Re < 2 \times 10^5$ else taken as turbulent flow.

If the flow is laminar, the skin friction coefficient is given as;

$$C_f = \frac{1.327}{\sqrt{Re}}$$

If the flow is turbulent, the skin friction coefficient is given as;

$$C_f = \frac{0.455}{(\log(Re))^{2.59}}$$

Where the Reynolds number,

$$Re = \frac{\rho V l}{\mu}$$

3.7.1.2. Form Factors

Wing and tail surfaces,

$$FF = \left[1 + \frac{0.6}{\left(\frac{x}{c}\right)_m} \left(\frac{t}{c}\right) + 100 \left(\frac{t}{c}\right)^4 \right], [1.34M^{0.18} \cdot (\cos\Delta_m)^{0.28}]$$

Fuselage,

$$FF = 1 + \frac{60}{f^3} + \frac{f}{400}$$

$$f = \frac{l}{d} = \frac{l}{\sqrt{\left(\frac{4}{\pi}\right) \cdot A_{max}}}$$

t/c = Thickness to chord ratio

x/c = Maximum thickness location on the chord (normalized to x-axis)

Δ_m = Maximum sweep angle

Table 4: C_{d_0} calculations

Component	Reynolds Number	Flow Characteristic	C_{D_0}
Wing	$< 2 \times 10^5$	Laminar	0.0062
	$> 2 \times 10^5$	Turbulent	0.0111
Fuselage	$> 2 \times 10^5$	Turbulent	0.0035
Horizontal Tail	$< 2 \times 10^5$	Laminar	0.0013
	$> 2 \times 10^5$	Turbulent	0.0021
Vertical Tail	$< 2 \times 10^5$	Laminar	0.0007
	$> 2 \times 10^5$	Turbulent	0.0012

3.7.2. Induced Drag

Induced drag is the drag that occurs in response to the Lift produced.

$$C_{D_i} = \frac{k * W^2}{q * S}$$

K = The induced drag correction factor

$$k = \frac{1}{\pi * e * AR}$$

'e' represents Oswald efficiency and is calculated with the formula below,

$$e = 1.78(1 - 0.045AR^{0.68}) - 0.64$$

3.7.3. Crud Drag

Crud drag is characterized as drag caused by leakages, protuberances, and other imperfections. Crud drag can be taken as 28 percent of $(C_{d_0} + C_{d_i})$ regardless of aircraft size, as Feagin and Morrison stated.

3.7.4. Thrust Calculation

$$F = 4,3923 \cdot 10^{-8} \cdot RPM \cdot \frac{d^{3,5}}{\sqrt{pitch}} \cdot (4,233 \cdot 10^{-4} \cdot RPM \cdot Pitch - v_0)$$

Due to competition requirements, AXI Gold 2826/10 engine and APC-E 10x6 propeller will be used in aircraft. According to Gabriel Staples Equation [4], 12N thrust will be obtained at 0 m/s by assuming about 16% of the efficiency loss of the engine. Cruise speed has been predicted as 13-14 m/s taking into account the decrease in thrust and increased drag force with increasing speed.

3.7.5. Drag and Thrust Calculation Results

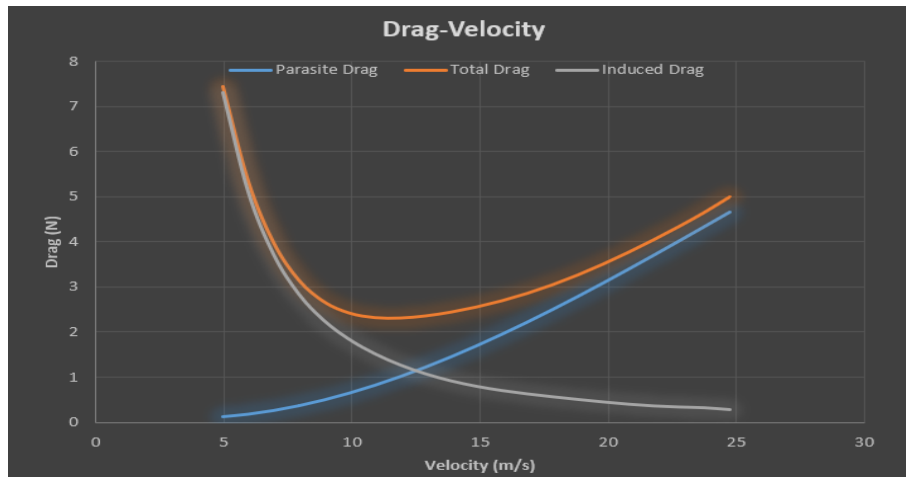


Figure 23: Drag versus Velocity Graph

The variation of induced drag and parasitic drag depend on the velocity that is used to estimate the region with minimum total drag.

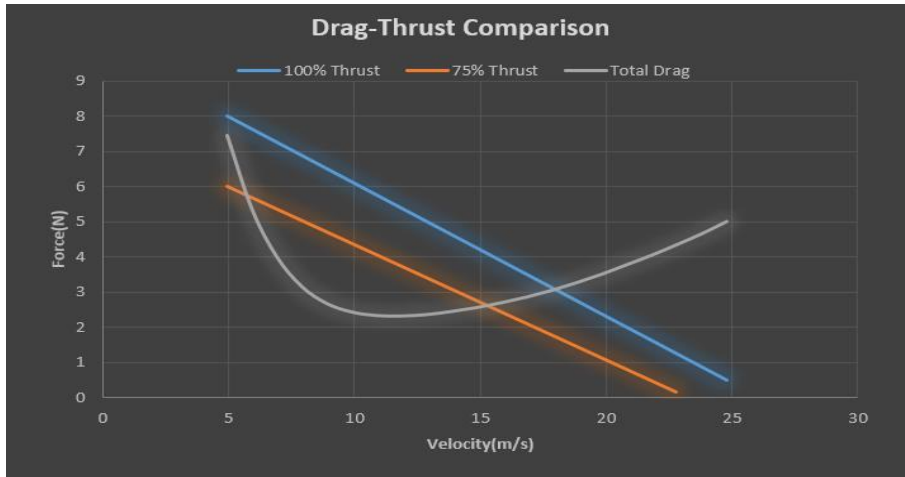


Figure 24: Drag-Thrust Comparison

The drag-thrust comparison graph was used to estimate the cruise speed.

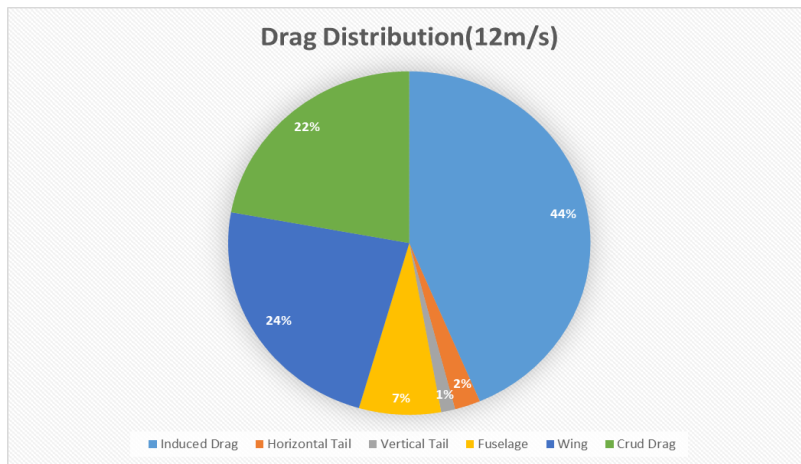


Figure 25: Contribution to drag of aircraft components

Distribution of drag forces that the aircraft will be exposed to at 12m/s, which is calculated as the minimum speed at which the minimum lift force is required for the aircraft to take off.

3.7.6 Verification of Wing Produced Lift and Drag

The parameters selected while designing the aircraft are close to the UAV's limits. To ensure that the UAV will fly, it must be confirmed whether it can produce the necessary lift force, and even whether the engine is strong enough to overcome drag force. Therefore, it seemed necessary to perform CFD analysis for more realistic results. The outputs of the CFD analysis for the lift and the drag are as follows;

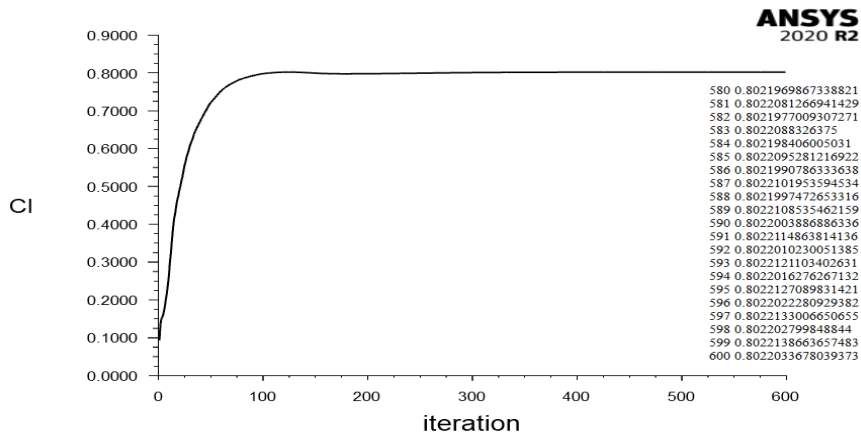


Figure 26: CFD Results for Cl calculation from ANSYS Fluent

We also have XFLR5 results for the 3D wing's lift coefficient. To compare the lift coefficient results both results are listed here.

Table 5: XFLR5 and ANSYS Fluent Comparison for Cl calculation

XFLR5	Ansyes Fluent	%error (XFLR5)
0.825335	0.802203	2.88

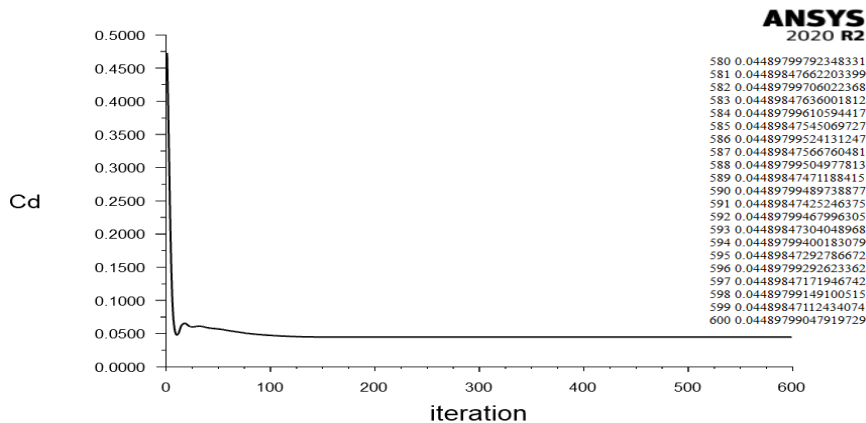


Figure 27: CFD Results for Cd calculation from ANSYS Fluent

Drag coefficient estimated with component build-up method to create Drag-Thrust figure. Moreover, the method's results gave an opinion to decide on cruise speed. However, for future calculations, it is better to work with more accurate sources. For this purpose, the 3D wing's drag coefficient was obtained from XFLR5 and Ansys Fluent.

Table 6: Comparison for C_{D0} calculations

Method/Source	C_{D0}	%error
XFLR5	0.041133	8.38
Component Build-Up	0.040806	9.11
Ansys Fluent	0.044898	-

As can be seen, the lift coefficient results are accurate but drag results are higher than estimated. On the other hand, if we consider that the UAV will fly at low speeds, this error will not make much difference in drag force. So, drag force results are still inside of the safety margin that we considered in the designing phase.

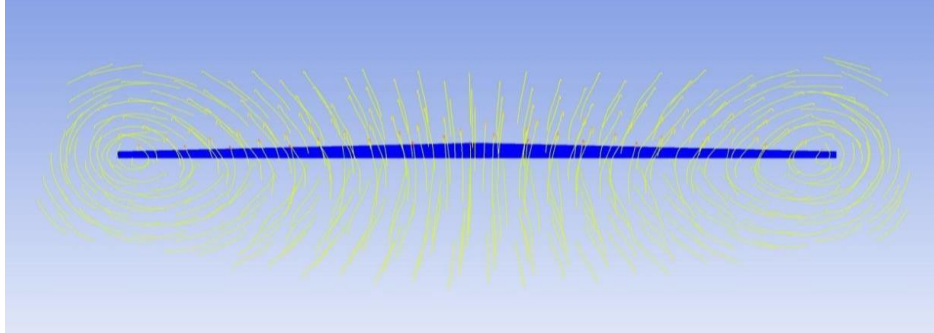


Figure 28: Streamlines for tip vortices from ANSYS Fluent

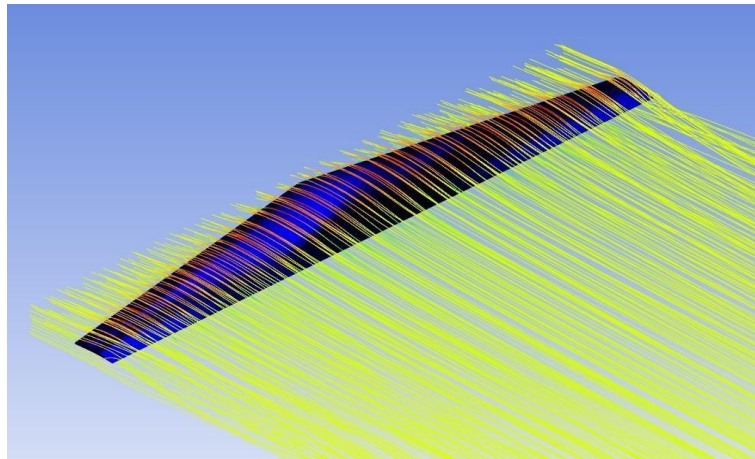


Figure 29: Streamlines on wing surface from ANSYS Fluent

4. STRUCTURAL DESIGN

4.1. Wing Structural Design

A total of fourteen ribs, two spars and two carbon pipes will be used in the internal structure of the wing. Ribs have functions such as transferring the aerodynamic loads on the skin to the structure, stability against buckling, and protection of the aerodynamic profile structure [5]. Due to the higher loads in the root part, the distance between the ribs is shorter and the thickness of the ribs to be positioned in this part is greater. As can be seen in Figure 2.1.1, the ribs shown in pale brown have a thickness of 4 mm, while the remaining ribs have a thickness of 3 mm. Ribs are planned to be produced from balsa.

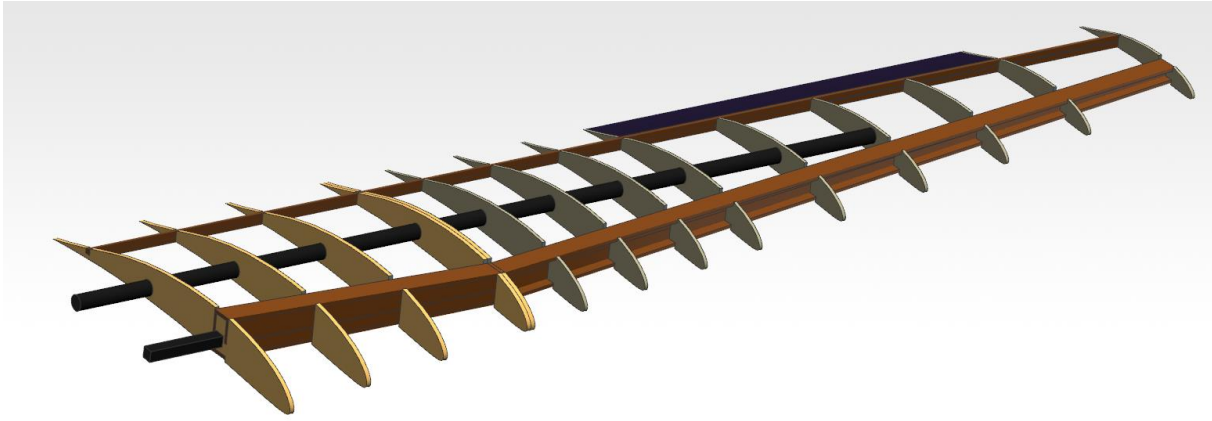


Figure 30: Wing Structure

One of the spars to be used in the internal structure of the wing will be placed at 25 percent of the chord length of the wing. The other will be placed just in front of the control surface. Spars are the main carrier elements of the wings. The reason for using two spars in the wing is to prevent bending. The two spars will both distribute the load and provide the torsional rigidity of the wing. Due to the sweep angle on the wing, the front spar will be produced as refracted. As can be seen in Figure 31, the front spar is placed to be compatible with the sweep angle of the wing from the fifth rib. Two different spar shapes will be used in the structure of the front spar. The carbon pipes in the front of the wing are to be used to fix the wing to the fuselage. In order to increase the rigidity of the structure, the upper flange and lower flange to be used in the front spar will be produced in one piece. Fastener and adhesive will be used for the connection of the fifth and the sixth ribs with each other. The rear spar is easing the connection of the aileron. In order to increase the strength of the wing, all spars will be produced in such a way that they are intertwined with ribs. For the manufacture of the front spar, birch plywood will be used. Balsa will be used for the rear spar.

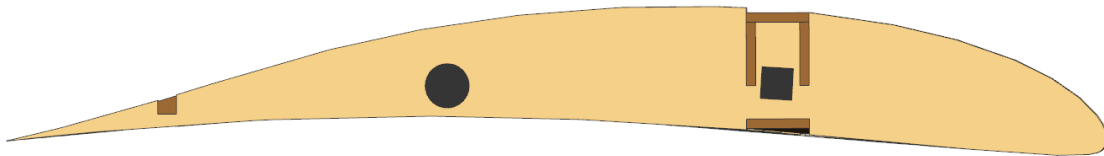


Figure 31: Fuselage Connection (Root Section)

As can be seen in Figure 32, four structures inside the wing will extend along the span. Two of them are the front and rear spars and the others are the carbon pipes. Square carbon pipe will be used on the front. This pipe was placed at an angle of 3.5 degrees while being placed. In this way, the tilt angle to be given to the wing will be provided while connecting the wing body. The round pipe to be used in the middle is larger than the square pipe. Wing body connection will be made by using these two pipes. Furthermore, these pipes will support the spar by carrying some of the aerodynamic forces. As can be seen in Figure 2.1.3, the connection

between the first and last rib will be made with spars. The carbon pipe to be used in the front will extend to the fifth rib, while the round carbon pipe to be used in the middle will extend to the eleventh rib.

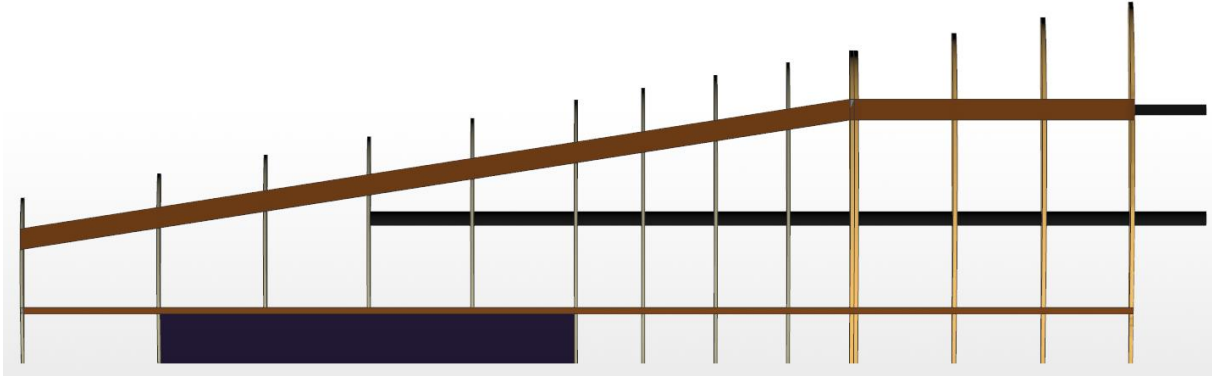


Figure 32: Connections View From Above

4.2. Tail Structural Design

The tail has a conventional configuration. It is planned that the tail will be designed in three parts and be detachable. The horizontal tail will be produced in two pieces, and the vertical tail in one piece. The horizontal tail contains two elevators, and the vertical tail includes a one-piece rudder. The rudder and elevators of the tail are connected to the fuselage with a carbon fiber pipe. Also, the ribs in both the horizontal stabilizer and the vertical stabilizer are attached with each other using the carbon pipes.

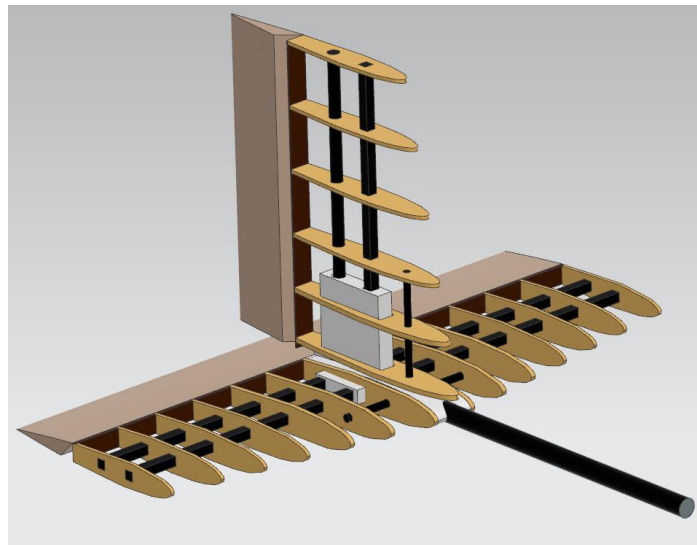


Figure 33: Tail internal structure and control surfaces

The connection of the elevator, rudder and carbon fiber pipe with the fuselage was provided with a 3-D printed component. The reason for the fitting to be printed from the 3D was the ease of use in the installation and removing processing.

PLA filament was used for the part printed from the 3D printer. The feature that distinguishes PLA from other filaments is that it is more accessible and easier to print. Unlike other filaments, PLA is completely natural and soluble.

The position of the last ribs connecting the piece in the rudder and elevator supports the connection between the horizontal tails, vertical tail and the 3D piece.

The carbon fiber pipes which hold the ribs in the rudder are inserted into the holes that open into the main pipe of the body. Moreover, the pipes passing through the horizontal and vertical tails are used to better fix the ribs and hold them together. In order to gain strength in the root, the ribs on the right and left roots are made thicker than the ribs on the ends.

4.3. Fuselage and Mechanical Systems

4.3.1. Fuselage

While choosing the material in the fuselage design, parameters such as durability, weight, ease of production and cost were evaluated. As a result of these evaluations, the durability and lightness of the material were the first criteria, while the ease of production and cost were also taken into consideration. As a result of the comparisons, it was decided to use carbon fiber reinforced composite as the main material for fuselage production. In addition, foam reinforcement will be made between carbon composites due to their light and flexible structure.

Table 7: Fuselage Material Selection

Parameters	Percentage (%)	Carbon Fiber	Fiber Glass	Kevlar	Balsa	Aluminum	Foam
Durability	40	5	4	5	1	4	2
Weight	30	3	2	4	5	2	4
Manufacturability	15	4	3	1	5	4	5
Cost	15	2	2	1	4	3	5
Total	100	3.8	2.95	3.5	3.4	2.95	3.5

4.3.2. Mechanical Systems

The same parameters were evaluated while choosing the material for the wing-tail and landing gear mechanisms that make up the mechanical systems.

4.3.3. Wings and Tail

Considering the low weight parameter for the wing, the use of balsa was emphasized. For the wing interior structure to have high durability, plywood was used as the front spar from the root to the tip, and carbon pipe was used as the rear spar.

For the tail design, importance was given to the lightness of the tail, so it was decided to use balsa. At the same time, carbon pipe is used to make the skeleton durable.

Table 8: Wing-Tail Material Selection

Parameters	Percentage (%)	Plywood	Balsa	Foam	Carbon Fiber
Durability	40	4	3	1	5
Weight	30	3	5	5	4
Manufacturability	20	4	5	4	3
Cost	10	3	3	5	1
Total	100	3.6	4	3.2	3.9

4.3.4. Landing Gear

The landing gear performs tasks such as carrying the main weight of the UAV and providing balanced movement on the ground. For this reason, importance was given to the durability and weight parameters in material selection. As a result of the evaluations, it was decided to use aluminum for both the front and rear landing gear.

Table 9: Landing Gear Material Selection

Parameters	Percentage (%)	Aluminum	Carbon Fiber	Plastic
Durability	40	4	5	1
Weight	30	3	4	5
Manufacturability	20	5	2	2
Cost	10	3	1	5
Total	100	3.8	3.7	2.8

4.4. Wing Structural Analysis

In the structural analysis section, finite element analysis was applied to the wing model. MSC Patran/Nastran were used for finite element analysis. According to plane stress theory, if the stress variation across the thickness of a structure is very small, it can be modeled in two dimensions. Due to this assumption, all of the internal structure parts are modeled as two-dimensional shell elements. In the material property section, for simplicity all materials are assumed as isentropic and average values of Young's modulus, Poisson's ratio and densities are used.

In the calculation of force acting on wing structure, the load factor value determined by the airworthiness authorities was used [6].

$$n = 2,1 + \left(\frac{24000}{W + 10000} \right) = 2,1 + \left(\frac{24000}{3352 + 10000} \right) = 3,9$$

$$\text{Total Lift Force} = (3.9) \times (9.81 \frac{m}{s^2}) \times (3.352 \text{ kg}) = 128.24 \text{ Newton}$$

The Schrenk method was used to calculate the approximate distribution of the lift force on the wing [7].

$$L'_{\text{Elliptical}} = \frac{4S}{\pi b} \sqrt{1 - \frac{2y^2}{b^2}}$$

$$L'_{\text{Planform}} = \frac{2S}{(1 + \lambda)b} \left(1 + \frac{2y}{b} (\lambda - 1) \right)$$

$$L'_{\text{Schrenk}} = \frac{L'_{\text{Elliptical}} + L'_{\text{Planform}}}{2}$$

S: Wing Area (m²)

λ: Taper Ratio

y: Distance to root (m)

b: Wing Span

After calculation of lift distribution over the wing, the force is adjusted to be applied from the middle of each two ribs. While transferring load to structure, RBE3 rigid connectors are used. RBE3 rigid connectors transferred loads to the internal structure from the stations determined in the structure.

Station Number	Distance to Root [m]	Surface Area [m ²]	Span [m]	Taper Ratio	L'Elliptical	L'Planform	L'Schrenk	Ratio	Applied Lift [N]
1	0.0425	1.09685	2.15	0.46728972	0.649051609	0.680735958	1.329787566	0.104658703	13.41201284
2	0.128	1.09685	2.15	0.46728972	0.644938403	0.65127332	1.296211723	0.102016173	13.07337255
3	0.2185	1.09685	2.15	0.46728972	0.636000321	0.620087721	1.256088041	0.098858306	12.66869187
4	0.299	1.09685	2.15	0.46728972	0.623928267	0.592348044	1.216276311	0.09572499	12.26715748
5	0.367	1.09685	2.15	0.46728972	0.610533774	0.56891577	1.179449544	0.092826601	11.89572894
6	0.437	1.09685	2.15	0.46728972	0.593467129	0.544794313	1.138261442	0.089584961	11.48031269
7	0.5045	1.09685	2.15	0.46728972	0.573585381	0.521534335	1.095119716	0.086189563	11.04519253
8	0.587	1.09685	2.15	0.46728972	0.544171578	0.493105474	1.037277052	0.081637153	10.46180119
9	0.687	1.09685	2.15	0.46728972	0.499607845	0.458646248	0.958254094	0.075417784	9.66478897
10	0.787	1.09685	2.15	0.46728972	0.442482925	0.424187023	0.866669948	0.068209807	8.741086744
11	0.8885	1.09685	2.15	0.46728972	0.365649771	0.389210909	0.754860679	0.059410046	7.61339734
12	1.006	1.09685	2.15	0.46728972	0.228966012	0.348721318	0.57768733	0.045465914	5.826456863
13	1.075	1.09685	2.15	0.46728972	0	0.0324944	0.0324944	0.002557417	0.327733031
Total								1	128.477733

Figure 34: Shrenk Approximation results and calculated lift distribution over wing

As seen in the Figure 35, approximate distribution of lift force was calculated. Then the ratio of distribution was calculated and applied to the total lift. Due to the last station which is wing tip, lift was slightly increased. Total lift force which is 128.477733 N is applied to the finite element model.

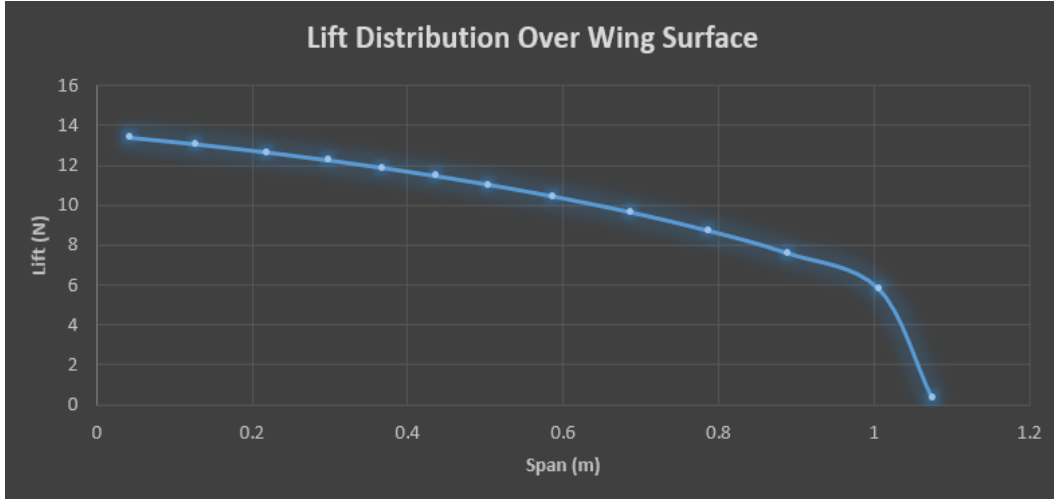


Figure 35: Lift distribution over wing surface for Schrenk Approximation

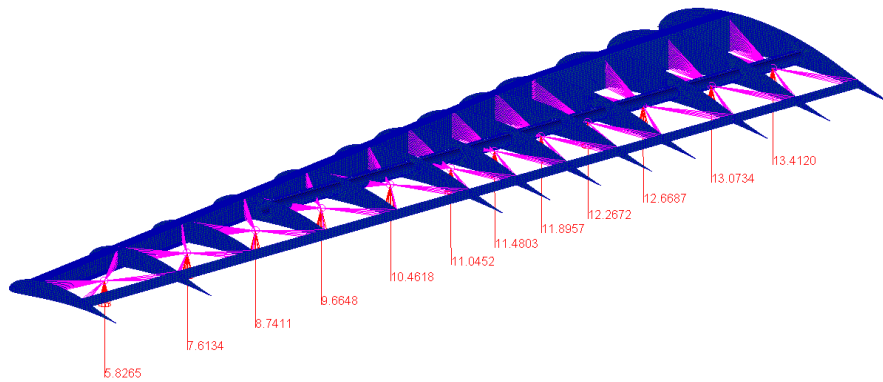


Figure 36: The Finite Element Model with Applied Forces in the MSC Patran

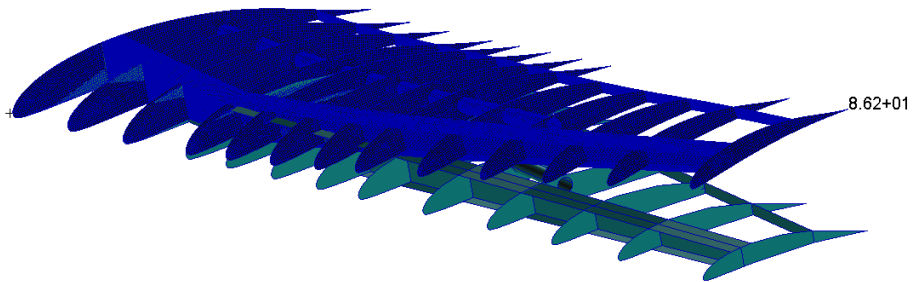


Figure 37: The displacement results for static analysis obtained by MSC NASTRAN

As a result of the static analysis, a deformation of 8 cm is expected in the structure as seen in Figure [38]. When the static tests specified in the production phase are applied to the structure, the experimental deformation that will occur in the structure will be determined.

5. AVIONICS

5.1. Batteries

Considering the regulations, our battery should be able to deliver more than 30A. The GensAce Li-Po battery with specs: 3S 2.5Ah 25C are chosen as the main battery to feed the ESC and motor. Maximum discharge rate is calculated as: $25C \times 2.5Ah = 62.5 \gg 30A$.

Assuming that we save a 20% capacity on the battery to avoid deterioration of the chemistry. Expected flight time at full throttle is:

$$t = \frac{\text{Battery available energy}}{\text{Discharge rate}} = 0,8 \cdot \frac{2.5Ah}{30A} = 0,0833 h = 5 min$$

In the regulation, a second battery was requested to feed the radio equipment. In this direction, a 2S 880 mAh Li-Po battery will be used.

5.2.ESC

Same as with the batteries the speed controller has to be able to deal with 30A continuous so we chose a 60A SKYWALKER ESC.

5.3. Connectors

XT60, which is a reliable choice for connector, will be used with motor and ESC connection.

5.4. Servos

The servos are chosen to actuate the differential ailerons and flaps, the rudder and elevator as well as the wheel steering have been Tower Pro SG-5010 RC Servo Motor.

5.5. Radio Control

Radiolink AT10 II controller with 2.4 GHz frequency value will be used as expected from us in the regulations.

6. PAYLOAD PREDICTION

As a result of the aerodynamic analysis, a lift force was estimated with the calculation based on the aircraft's lift coefficient at 0 angle of attack (0.775) and the average weather conditions of the region where the competition will be held. While this calculation, cruise speed was accepted as 12 m/s and air density at nearly 620 meter altitude (altitude of Munich + 100m) was calculated as 1.13146 kg/m³. If the lift equation is applied to these values, 34.63 Newton (3.53 kg) lift force will be obtained.

$$Lift(N) = W_{Aircraft}(N) + W_{Payload}(N)$$

The weight of aircraft without a payload is 2.122 kg. It is seen that approximately 1.4 kg payload can be carried as a result of subtracting the weight of the aircraft from the lift force obtained. Safety margin was used as taking into account the problems that may arise during the competition and the total payload was determined as 1.2 kg.

$$W_{Payload}(N) = 34.63 - 20.81682 = 13.813N$$

$$y = 3,12x - 2,122$$

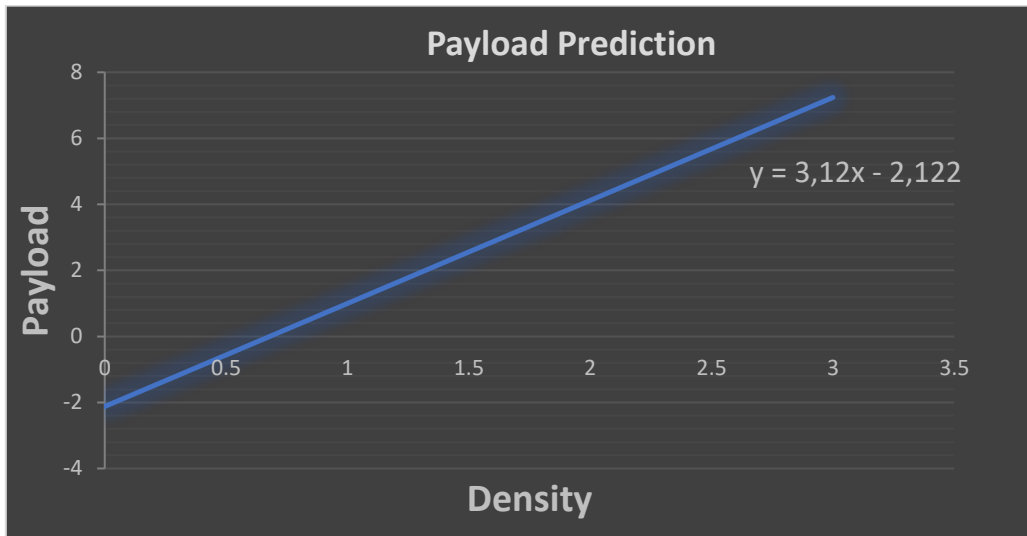


Figure 38: Payload prediction graphic

7. OUTLOOK

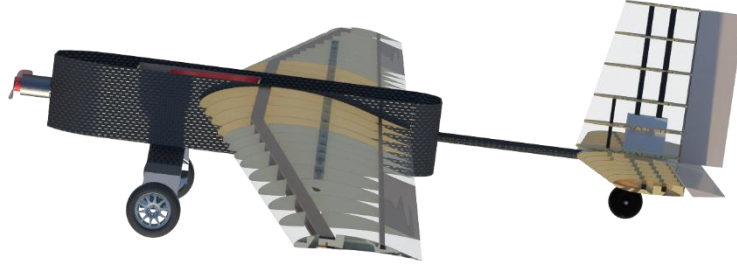


Figure 39: Side view of final aircraft

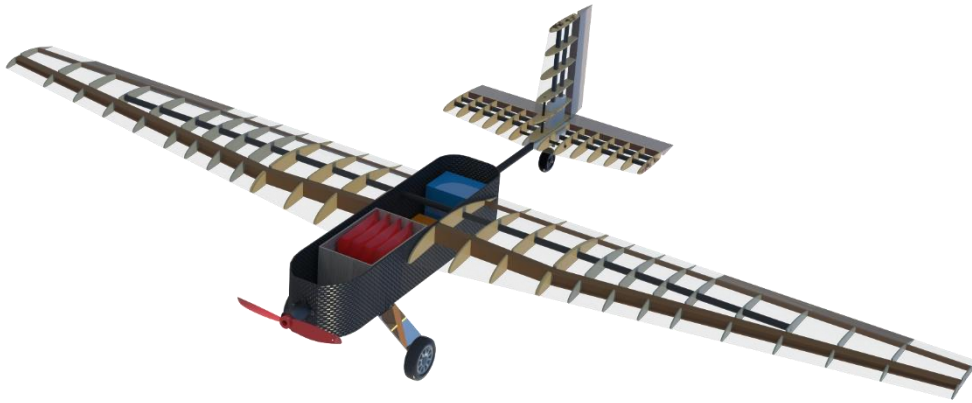


Figure 40: Isometric view of final aircraft

In preliminary design phase, the competition requirements were analyzed and the final design emerged as a result of the researches. Tapered overhead wing, conventional tail and tail-dragger landing gear were chosen as the final configuration. Then the structure is sized as a result of detailed drag and lift analysis. Finally manufacturing process has started according to the determined design.

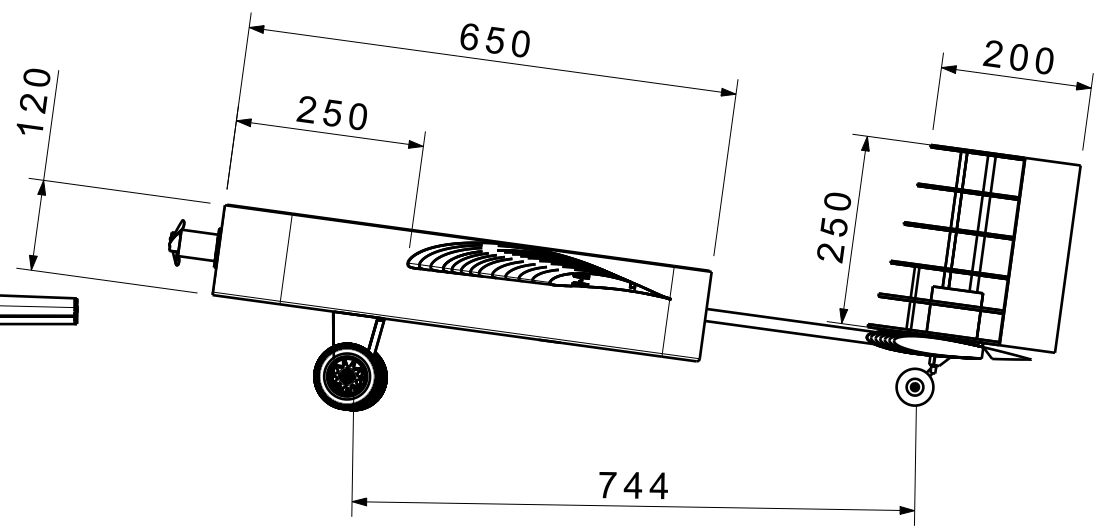
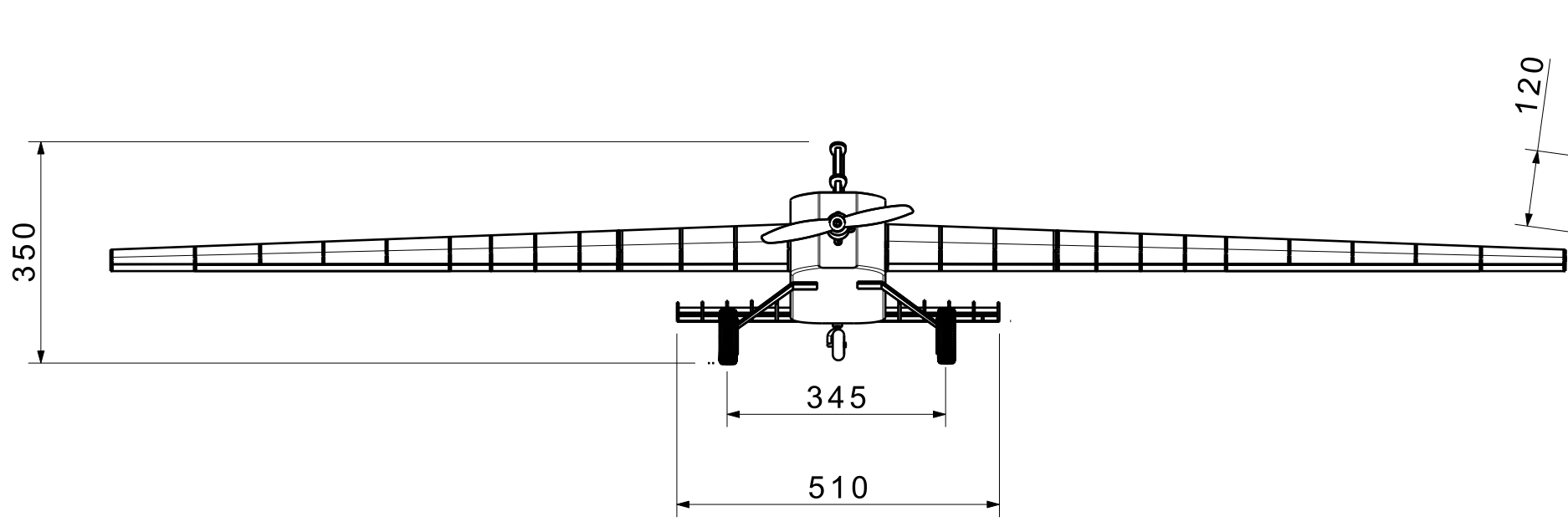


REFERENCES

- [1] Yechout, M. "Introduction to Aircraft Flight Mechanics", AIAA Education Series, 2003
- [2] Sadraey, M. "Aircraft Design: A Systems Engineering Approach" 2013
- [3] Feagin, R. C., & Morrison, W. D. "Delta method, an empirical drag buildup technique". NASA. 1978
- [4] Staples, G. "Propeller Static & Dynamic Thrust Calculation" 2014
- [5] Raymer, Daniel P., "Aircraft design: A conceptual approach" , 2nd ed., AIAA Education Series, AIAA, Washington, DC, 1992
- [6] Megson, THG. "Aircraft Structures for Engineering Students" 1999
- [7] Schrenk, O. "A simple approximation method for obtaining the spanwise lift distribution." 1941

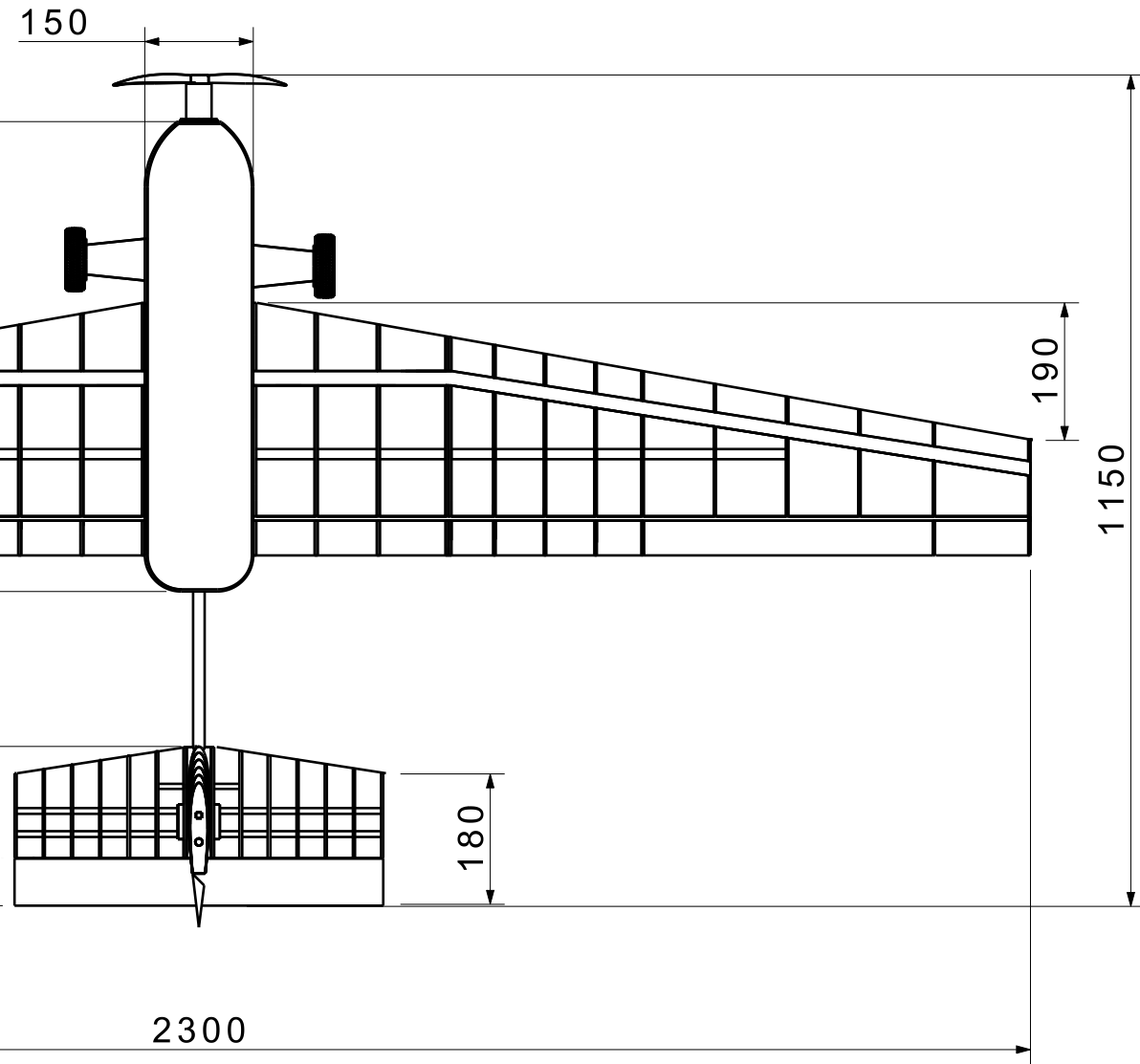
H G F E D C B A

4



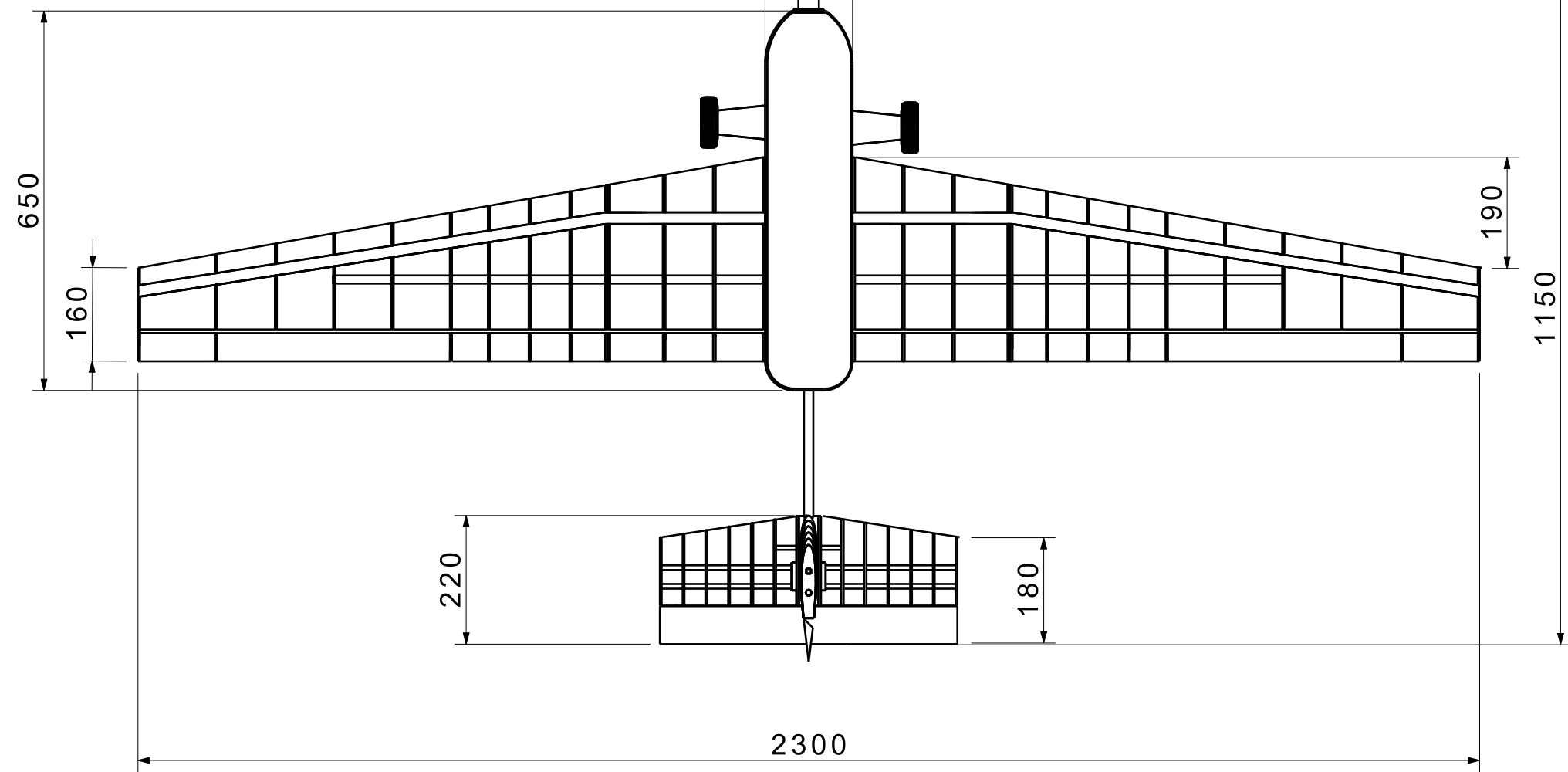
4

3



3

2



2

1

Size	A3		
Drawing Dimesions	mm		
	ISTANBUL TECHNICAL UNIVERSITY		
	SKY UAV TEAM		
Properties	Wing	Horizontal Tail	Vertical Tail
Airfoil	Dae 31	NACA 0012	NACA 0012
Span mm	2150	510	250
Aspect Ratio	8.43	2.55	2.22
Taper Ratio	0.46	0.81	1.25
Area cm2	5484	1020	281.25

1

H G B A

H G F E D C B A

4

4

3

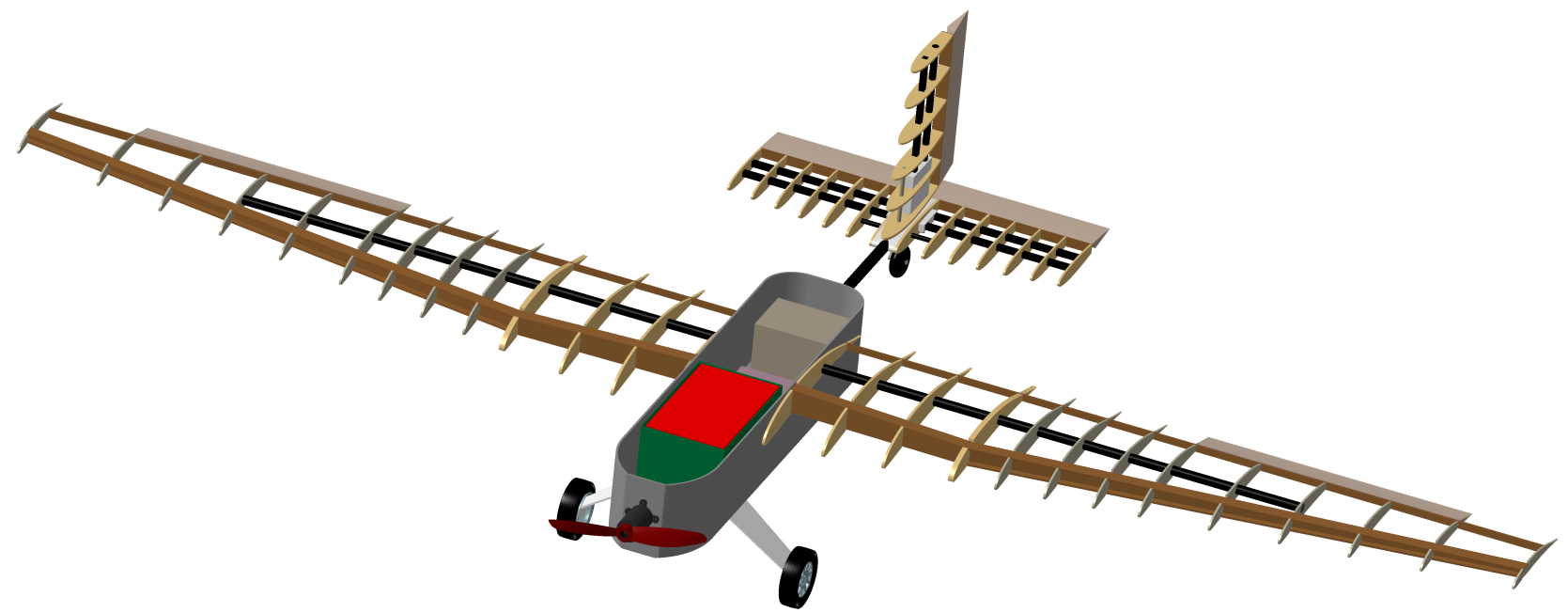
3

2

2

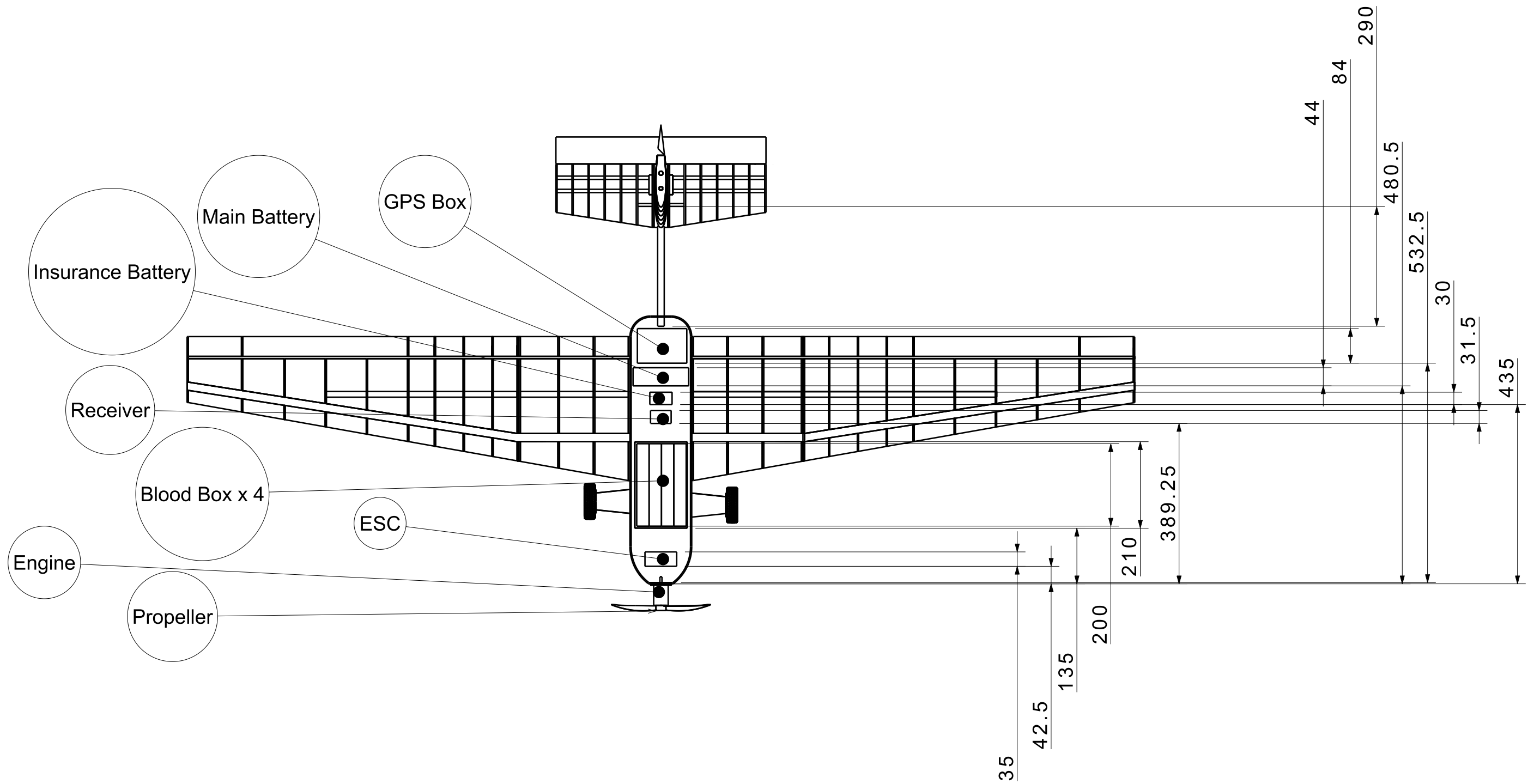
1

1



ISOMETRIC VIEW	
Size	A3
Drawing Dimesions	mm
ISTANBUL TECHNICAL UNIVERSITY	
SKY UAV TEAM	

H G B A



Equipment Locations	
Size	A3
Drawing Dimension	mm
ISTANBUL TECHNICAL UNIVERSITY	
SKY UAV TEAM	